JACS
JOURNAL OF THE AMERICAN CHEMICAL SOCIETY
Article
pubs.acs.org/JACS

Specificity of Growth Inhibitors and their Cooperative Effects in Calcium Oxalate Monohydrate Crystallization

Sahar Farmanesh,[†] Sriram Ramamoorthy,[‡] Jihae Chung,[†] John R. Asplin,[§] Pankaj Karande,[‡] and Jeffrey D. Rimer*,[†]

[†]Department of Chemical and Biomolecular Engineering, University of Houston, Houston, Texas 77204, United States
[‡]Department of Chemical and Biological Engineering, Rensselaer Polytechnic Institute, Troy, New York 12180, United States
[§]Litholink Corporation, Laboratory Corporation of America Holdings, Chicago, Illinois 60612, United States

Supporting Information

ABSTRACT: The molecular recognition and interactions governing site-specific adsorption of growth inhibitors on crystal surfaces can be tailored in order to control the anisotropic growth rates and physical properties of crystalline materials. Here we examine this phenomenon in calcium oxalate monohydrate (COM) crystallization, a model system of calcification with specific relevance for pathological mineralization. We analyzed the effect of three putative growth inhibitors—chondroitin sulfate, serum albumin, and transferrin—using analytical techniques capable of resolving inhibitor–crystal interactions from interfacial to bulk scales. We observed that each inhibitor alters surface growth by adsorbing on to distinct steps emanating from screw dislocations on COM surfaces. Binding of inhibitors to different crystallographic faces produced morphological modifications that are consistent with classical mechanisms of layer-by-layer crystal growth inhibition. The site-specific adsorption of inhibitors on COM surfaces was confirmed by bulk crystallization, fluorescent confocal microscopy, and atomic force microscopy. Kinetic studies of COM growth at varying inhibitor concentrations revealed marked differences in their efficacy and potency. Systematic analysis of inhibitor combinations, quantified via the combination index, identified various binary pairings capable of producing synergistic, additive, and antagonistic effects. Collectively, our investigation of physiologically relevant biomolecules suggests potential roles of COM inhibitors in pathological crystallization and provides guiding principles for biomimetic design of molecular modifiers for applications in crystal engineering.

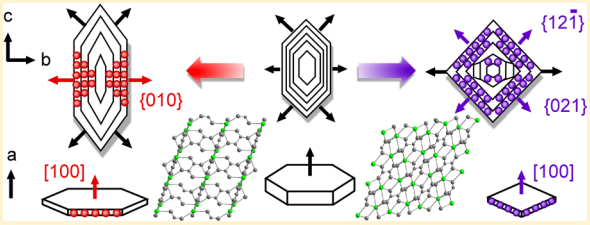

INTRODUCTION

The interactions between ions or molecules with crystalline interfaces play an integral role in many natural and synthetic processes yielding materials with unique, often exquisite, structural properties. Broadly categorized, these modifiers (or inhibitors) interact with crystal surfaces via a range of intermolecular forces, such as van der Waals, hydrogen bonds, ionic bonds, or in rare cases covalent bonds. One of the challenges associated with identifying effective modifiers is the ability to characterize the physicochemical factors regulating their specificity for binding to distinct crystallographic faces. Harnessing the ability to tune such interactions affords opportunities to both understand phenomena in living systems and foster translational approaches in the rational design of novel materials.

Growth inhibitors bind to specific faces of crystals and frustrate the attachment of solute molecules, thereby reducing the rate of crystal growth normal to the surface. Crystals generally grow by classical mechanisms involving two-dimensional (2D) layer nucleation and spreading via the advancement of steps across crystal planes. Growth inhibitors exhibiting site specificity for faces of crystals impede step advancement and alter the rate of anisotropic growth. Inhibitor–crystal interactions can be designed to tailor crystal size, habit, or surface architecture. There are numerous examples of such processes in nature, which include the formation of calcium carbonate in nacreous shells,[1] calcium phosphate in bone,[2] and the siliceous (amorphous) exoskeleton structures of unicellular organisms (e.g., sponges and diatoms).[3,4] These processes are mediated by the interaction of modifiers (mostly proteins) with surfaces of biogenic materials. In some instances, the native function of modifiers is that of an inhibitor intended to suppress crystallization. Examples include antifreeze proteins (AFPs) that prevent ice formation in cold weather species,[5] biomimetic analogues of proteins (e.g., peptoids),[6,7] and drugs for infectious diseases (e.g., hemozoin crystals in malaria-infected red blood cells)[8] or pathological diseases (e.g., calcium crystals in renal stones).[9−11] It is important to emphasize that inhibitor–crystal interactions are not restricted to biological systems, but are also evident in synthetic crystallization. Notable examples include modifiers of organic crystals,[12,13] zeolites,[14,15] minerals,[16−19] and metal oxides.[20]

Received: October 16, 2013
Published: December 6, 2013

dx.doi.org/10.1021/ja410623q | J. Am. Chem. Soc. 2014, 136, 367−376

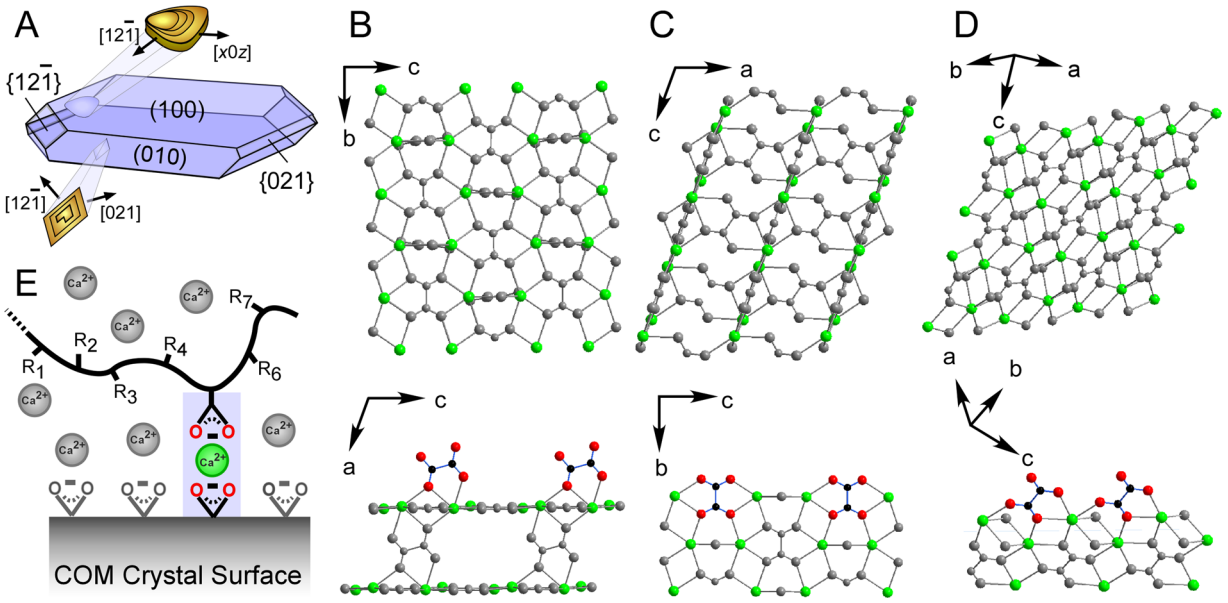

Figure 1. (A) The morphology of COM crystals. (B–D, top row) Cross-sectional images normal to each crystallographic plane highlight topologies of the (B) (100), (C) (010), and (D) (12-1) faces. Here we emphasize the spatial arrangement of calcium ions (green) on each crystal surface. Oxalates are shown in gray, and water molecules are omitted for clarity. (B–D, bottom row) Views oriented parallel to each crystal plane (i.e., orthogonal to images on the top row). Surfaces were cleaved to depict two oxalate molecules in the crystal lattice (oxygen = red, carbon = black). The orientation of oxalate molecules relative to the plane of each crystal face is different. It is reasonable to expect that the alignment of oxalate molecules may reflect the preferred orientations of carboxylic acid moieties of the inhibitors adsorbed on COM crystal faces. (E) COM growth inhibitors are rich in carboxylic acid groups that mimic oxalate vacancies on COM crystal surfaces. These anionic moieties bind to COM interfaces via calcium bridges: $_{(COM)}COO^{-}\cdots Ca^{2+}\cdots{}^{-}OOC_{(inhibitor)}$.

In this study we focus on growth inhibition of calcium oxalate monohydrate (COM), which is the primary constituent of human kidney stones.[21] The organic matrix of COM renal stones is comprised of proteins, polysaccharides, carbohydrates, lipids, and other biomolecules.[22] Proteomics studies of human stone matrix reveal over 60 unique constituents[23] with 9 proteins found in all types of stones.[24] Many of these matrix proteins are putative inhibitors of COM formation. A common observation is that effective inhibitors of COM crystallization contain a high percentage of anionic groups.[9,25] This is evident among frequently studied urinary proteins, such as osteopontin (OPN),[26] and has also proven to be true for a variety of organic acids,[9,27,28] proteins, and peptides that are rich in carboxylic acid moieties (e.g., glutamic acid and aspartic acid).[25,29−34]

Herein, we examine three putative inhibitors of COM crystallization: chondroitin sulfate, serum albumin, and transferrin. We systematically quantify their efficacy and identify their site specificity for COM {12-1}, {021}, and (010) surfaces, which constitute the fastest growth directions of COM crystals. At a macroscopic (i.e., crystal) level, we find that inhibitors modulate bulk size and habit. Using atomic force microscopy (AFM) to monitor growth *in situ*, we provide microscopic validation of inhibitor interactions with COM surfaces that are consistent with the morphological changes observed in bulk crystallization studies. Moreover, kinetic studies of COM growth reveal marked differences in inhibitor efficacy. We extended this analysis to include binary combinations of inhibitors and observed pairings that display synergistic and antagonistic effects in COM growth inhibition. Collectively, the results of this study provide a benchmark for the biomimetic design of crystal growth inhibitors for applications such as drug design, while offering insights into potential growth inhibition mechanisms in pathological biomineralization.

EXPERIMENTAL SECTION

Materials. The following reagents for COM crystallization were purchased from Sigma Aldrich (St. Louis, MO) and used without further purification: calcium chloride dihydrate (ACS Reagent, 99+%), sodium oxalate ($Na_2C_2O_4$, >99%), albumin from bovine serum (lyophilized powder, ≥98%), albumin from human serum (lyophilized powder, ≥96%), human transferrin (bioreagent, ≥98%), chondroitin sulfate A sodium salt from bovine trachea (bioreagent, lyophilized powder), and sodium citrate dihydrate ($Na_3C_6H_5O_7{\cdot}2H_2O$, ≥99%). Fluorescent labeled albumin from bovine serum (Alexa Fluor 488 and 633 conjugate) and holo transferrin (Tf) from human serum (Alexa Fluor 488 and 647 conjugate) were purchased from Invitrogen (Carlsbad, CA). Sodium chloride (99.9% ultrapure bioreagent) was purchased from JT Baker (Center Valley, PA).

COM Crystallization. Stock solutions of calcium chloride and sodium oxalate were prepared at 10 mM concentration by dissolving appropriate quantities of each reagent in deionized water. A 20 mL solution of composition 0.7 mM $CaCl_2$:0.7 mM $Na_2C_2O_4$:150 mM NaCl was prepared in a clean glass vial by first dissolving NaCl in deionized water, then adding 10 mM $CaCl_2$ stock solution. The sample vial was placed in an incubator at 60 °C for 1 h prior to adding 10 mM $Na_2C_2O_4$ stock solution dropwise while stirring. Crystals prepared by this method are referred to herein as the control. COM crystallization in the presence of growth inhibitors was performed by adding an appropriate amount of inhibitor to achieve the desired concentration. Inhibitors were added to the solution prior to the addition of $Na_2C_2O_4$. All solutions were placed in the incubator at 60 °C for 3 days. A clean glass slide was placed at the bottom of the synthesis vial to collect crystals for analysis by microscopy. The glass slides were removed from the mother liquor, gently washed with deionized water to remove the residual supernatant, and dried in air prior to analysis. The pH of growth solutions with inhibitor(s) was measured before and after COM crystallization using an Orion 3-Star

dx.doi.org/10.1021/ja410623q | J. Am. Chem. Soc. 2014, 136, 367−376

Plus pH benchtop meter and 8102BNUWP ROSS Ultra electrode (see Table S1).

Herein we refer to COM crystals using the $P2_1/c$ space group with cell parameters a = 6.290 Å, b = 14.580 Å, and c = 10.116 Å (β = 109.46°).[35] The COM crystal habit is an elongated hexagonal platelet bounded by {100}, {010}, {12-1}, and {021} surfaces (Figure 1A). COM crystals differ with respect to the density and spatial arrangement of calcium ions as well as the orientation of oxalate groups relative to the crystal plane. Figure 1 presents the topology of COM crystal surfaces at angles normal to each crystal plane (panels B–D, top row) and perpendicular views (panels B–D, bottom row).

Bulk Crystallization Studies. The dimensions of COM crystals along the [010] and [001] directions were measured by optical microscopy using a Leica DM2500-M microscope equipped with Olympus objectives. COM crystals collected on glass microscope slides were imaged in reflectance mode and recorded with a DM2500-M video camera. The [100] thickness of COM bulk crystals was assessed by scanning electron microscopy (SEM) using a FEI 235 Dual-Beam Focused Ion Beam instrument equipped with SEM sample extraction probe. COM crystals on glass slides were transferred to carbon tape by gently pressing the slide to the tape. Samples were coated with a layer of mixed Pd and Pt (~15 nm) to reduce the effects of electron beam charging. Fluorescent microscopy was performed with COM control crystals. Alexa Fluor conjugated BSA and Tf protein (20 μg/mL) were dissolved in a supersaturated solution of 3.4 mM $CaCl_2$ and 0.17 mM $Na_2C_2O_4$ and incubated with crystals for 3 h at 37 °C. After incubation, the slides were washed three times with a saturated calcium oxalate (CaOx) solution to remove any unbound protein. The slides were imaged using an Olympus IX 81 fluorescence microscope with a Hamamatsu digital camera. Images of the crystals were obtained using a Zeiss LSM Meta 510 confocal microscope. A 488 nm argon laser and 633 nm helium neon laser were used to excite Alexa 488 and 633 labeled proteins, respectively. A band-pass filter (505–530 nm) and long pass filter (650 nm) were used to visualize the emission of 488 and 633 labeled proteins, respectively. Images were obtained using a 63× oil immersion objective (NA: 1.4).

Analysis of Protein Structure. The secondary structure of proteins was characterized by circular dichroism (CD) spectroscopy using an Olis rapid-scanning monochromator (RSM 1000). Protein solutions were prepared by adding 150 mM NaCl, 0.7 mM $CaCl_2$, and 25 μg/mL of either BSA or Tf. The CD spectrum for each protein was collected at both 25 and 60 °C to mimic conditions used for kinetic measurements and bulk crystallization assays, respectively.

Interfacial Studies. COM crystal surfaces were analyzed by AFM. Samples were mounted on AFM specimen disks (Ted Pella, Inc.) covered with a thin layer of photocurable epoxy (Lens Bond Type SK-9). Crystals were transferred to the AFM sample by gently pressing the glass microscope slide on the partially cured epoxy (pretreated with UV light for 60 min). The sample was placed under UV light for an additional 1 h to fully cure the epoxy and anchor COM crystals with either the (100) or (010) surface oriented in the plane of imaging. COM crystals were imaged with Olympus AC240TS cantilevers. The distribution of COM (100) step heights was assessed by scanning multiple areas of more than 10 crystals prepared from 3 separate crystal batches. For topographical imaging, we used an Asylum MFP-3D-SA instrument (Santa Barbara, CA) in contact mode (256 lines/scan and 1 Hz). For *in situ* measurements of COM (010) surface growth, we used a Nanoscope IV (Digital Instruments, Santa Barbara, CA) in contact mode at a scanning rate of 7 Hz. A growth solution of composition 3.6 mM $CaCl_2$:0.18 mM $Na_2C_2O_2$:150 mM NaCl (with supersaturation ratio S = 2.9) was introduced into the AFM liquid cell at a rate of 0.2 mL/min using a dual syringe pump (CHEMYX Fusion 200) with an in-line flow mixing configuration that combined separate stock solutions of calcium and oxalate just prior to entering the liquid sample cell.

Kinetic Studies. The kinetics of COM bulk crystallization was measured *in situ* using a calcium ion-selective electrode (ISE) from Orion (model 9720BNWP). COM growth was analyzed at 23 ± 2 °C using solutions of composition 0.5 mM $CaCl_2$:0.5 mM $Na_2C_2O_4$:150 mM NaCl (S = 4.1) with continuous stirring. For these studies, we selected a stirring rate of 1200 rpm (Figure S4A). We tested for potential CO_2 uptake from the atmosphere[36] (Figure S4B). Prior to each measurement, the ISE electrode was calibrated with calcium standards prepared by first diluting a commercial calcium solution (0.1 M, Orion Ion Plus) in deionized water to three different concentrations (10^{-1}, 10^{-2}, and 10^{-3} mol Ca^{2+}/L), then adding an ion strength adjuster (ISA, Thermo Scientific) in a 1:50 volume ratio of ISA-to-standard.

RESULTS AND DISCUSSION

Inhibitors of COM Crystallization. Proteomics studies of human renal stones reveal the presence of numerous ubiquitous species residing within the organic matrix.[23] Here, we analyzed several common matrix constituents (see Table 1) that have net negative or near neutral charge in COM growth solutions prepared at physiological pH (~ 6.1).[37] Anionic macromolecules tend to be very effective COM growth inhibitors. Past studies have focused on a select number of urinary proteins, such as nephrocalcin (NC)[38] and OPN.[25,33,34] The interactions between proteins transferrin (Tf)[39] and serum albumin (from bovine, BSA)[40] and the glycosaminoglycan chondroitin sulfate A (C_4S)[41] with COM crystals have been reported previously; however, few studies have systematically assessed their ability to inhibit COM crystallization. To this end, we focus our study on these three putative inhibitors.

Table 1. Comparison of COM Crystal Growth Inhibitors

crystal inhibitors	x (%)[a]
chondroitin sulfate A, C_4S	42 ± 6
serum albumin (bovine), BSA	36 ± 6
serum albumin (human), HSA	35 ± 6
citrate	30 ± 3
transferrin, Tf	11 ± 5

[a]Percent inhibition (eq 1) from ISE studies using 20 μg/mL inhibitor (i.e., onset of plateaus in Figures 4 and 7) in a solution with 0.5 mM CaOx and 150 mM NaCl (S = 4.1) at 25 °C.

The rate of COM crystallization was measured *in situ* using a supersaturated calcium oxalate solution and ISE to monitor the gradual depletion of free Ca^{2+} ions during crystal growth. ISE has proven to be a facile method for quantifying COM growth inhibition. A common approach is the constant composition method, which employs COM seeds suspended in a growth solution at low, constant calcium oxalate supersaturation (ca. S = 1.3).[36,42] Here, we used nonseeded growth solutions at high supersaturation (S = 4.1), which we previously demonstrated to be a rapid and reliable high-throughput diagnostic platform for assessing COM growth inhibitors.[10] Representative ISE curves in Figure 2A reveal the temporal consumption of free Ca^{2+} ions during COM growth in the presence of BSA (see Figure S6 for similar analyses with C_4S and Tf). The rate of crystal growth was assessed from the slope of ISE curves during the first 40 min of crystallization, which are approximately linear (note that these curves deviate from linearity as time progresses due to decreasing CaOx supersaturation; see Figure S4).

The efficacy of COM growth inhibitors was quantitatively assessed using the percent inhibition defined as:

$$x = \left(1 - \frac{r_{\text{inhibitor}}}{r_{\text{control}}}\right) \times 100\% \quad (1)$$

where r is the rate of Ca^{2+} consumption (ppm/min) assessed as the slope of ISE curves. Table 1 lists each inhibitor with

dx.doi.org/10.1021/ja410623q | J. Am. Chem. Soc. 2014, 136, 367–376

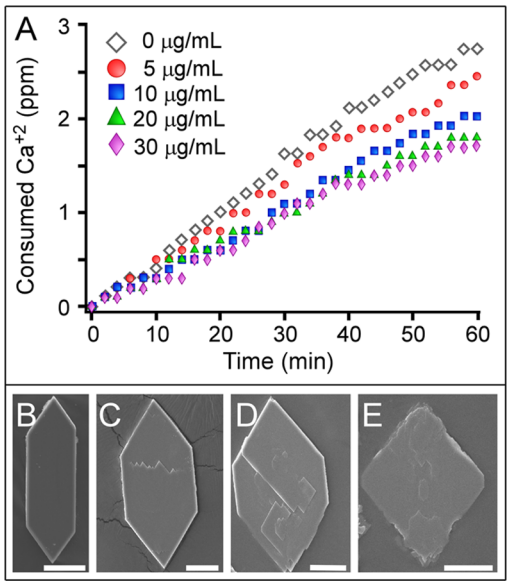

Figure 2. (A) Calcium ISE measurements of COM crystallization at 23 ± 2 °C in the presence of BSA at varying concentrations. The consumption of Ca^{2+} ions was measured in supersaturated solutions containing 0.5 mM CaOx and 150 mM NaCl. (B–E) SEM images of COM crystals prepared with increasing BSA concentration: (B) 0, (C) 5, (D) 10, and (E) 20 μg/mL. Scale bars = 20 μm.

corresponding x evaluated at a fixed inhibitor concentration, 20 μg/mL. The biomolecules selected for this study exhibit isoelectric points spanning from 3 to 7 (i.e., highly anionic to weakly cationic). The efficacy of anionic inhibitors has been validated for a variety of proteins,[9,25,28,34,42−47] organic molecules,[9,28,44,48,49] and polyelectrolytes.[50] A general trend observed among COM growth inhibitors is the increased percent inhibition with a higher percentage of negatively charged functional moieties. Moreover, small molecules, such as citrate, tend to be moderate inhibitors of COM crystallization, whereas macromolecules (e.g., proteins) tend to be more potent.[50]

The most effective inhibitor in this study was C_4S (x = 42 ± 8%), which is a glycosaminoglycan with several functional moieties capable of interacting with COM crystal surfaces, including anionic groups (i.e., carboxylic acid and sulfate) and hydrogen-bonding groups (i.e., alcohol, amide, and ester). A slightly less effective inhibitor was BSA (x = 36 ± 6%), which is a large protein (69 kDa) consisting of 5.9% Asp and 10.2% Glu amino acids. The secondary structure of BSA (Figure S1) consists of numerous α-helices, which was confirmed by CD spectra (Figure S3). Prior studies of COM crystallization report different sources of serum albumin, most notably from human (HSA) or bovine. The amino acid sequence and secondary structure of HSA (Figure S1) are similar to those of BSA. ISE measurements in COM growth solutions containing HSA resulted in nearly identical percent inhibition as BSA (see Table 1). Moreover, bulk crystallization studies revealed no apparent differences in COM crystal habit from either source of serum albumin (Figure S7). Here, we used BSA for all analyses.

The least effective inhibitor in this study was Tf, which is a common urinary protein (80 kDa) containing 6.3% Asp and 6.2% Glu amino acids, and numerous α-helices (Figure S2). ISE measurements revealed that Tf is a weak inhibitor of COM growth (x = 11 ± 5%), which can be partly attributed to the few anionic moieties in its amino acid sequence relative to BSA. As a benchmark, we compared all three inhibitors to citrate, which is a moderate growth inhibitor administered in renal stone treatment. The efficacy of citrate (x = 30 ± 3%) was comparable to BSA but less than that of C_4S. Collectively, these observations allude to a more generalized observation that inhibitor efficacy is not only solely attributed to net charge but also to a combination of influential factors that include (but are not limited to) local charge, composition, secondary structure, and the spatial positioning of amino acids.

COM crystal surfaces grow by the classical mechanism of layer nucleation and spreading from screw dislocations.[9,29,36,50] Growth inhibitors that bind to specific crystal faces reduce the rate of growth normal to the surface and can impede step advance within the plane of adsorption by step pinning.[9] Small changes in the inhibitor structure or composition, such as a switch from an Asp to Glu amino acid, are capable of inducing substantial changes in inhibitor efficacy. Indeed, prior studies of COM and other calcium minerals (e.g., calcium carbonate and calcium phosphate) have shown that subtle changes in the sequence or length of peptides[10,25,34,36,51−57] or peptoids[6] markedly impact their performance as crystal inhibitors. Notable examples include polyelectrolytes, such as poly aspartic acid[25,50] and poly(acrylic acid),[29,32] which preferentially bind to COM {12-1} faces, while the molecular analogue poly glutamic acid specifically binds to the COM (010) face.[25,50]

There are notable discrepancies in the literature regarding the site specificity of C_4S, BSA (or HSA), and Tf for COM crystal surfaces. Cook et al. used fluorescently labeled proteins in scanning confocal microscopy (SCM) studies to propose that HSA preferentially binds to the (010) face.[58] Sheng et al. used chemical force microscopy to assess the change in adhesion force between modified AFM tips in contact with COM surfaces in saturated CaOx solutions.[39] The force of adhesion between COOH-modified AFM tips (i.e., mimics of anionic amino acid moieties) and COM crystal surfaces in the presence of each inhibitor was compared to inhibitor-free solutions. Their studies suggest that BSA binds nonspecifically to all COM faces, C_4S interacts uniquely with (010) and {12-1} faces, and Tf interacts with (100) and {12-1} faces. Another study by Gul and Rez examined the number of calcium bridges formed between anionic amino acids of stone matrix proteins and calcium ions on idealized COM crystal surfaces. Using molecular dynamic simulations with rigid 3D protein structures determined from X-ray diffraction, they report the shortest protein–crystal contact length (i.e., most stable interaction) between Tf and the COM (12-1) face.[59] As we discuss herein, our findings differ from nearly all of these site-specific assignments for BSA, C_4S, and Tf.

We used a combination of microscopy techniques to examine the site-specific binding of BSA, C_4S, Tf, and citrate to COM crystallographic faces. Control crystals exhibit a hexagonal platelet morphology expressed by {100}, {010}, and structurally equivalent {12-1} and {021} faces (see Figures 1 and 3A). We used optical micrographs to measure the length-to-width aspect ratio (c/b) of COM crystals, and scanning electron micrographs to measure the [100] thickness. SEM images in Figure 2 reveal the progressive change in COM crystal habit with increasing BSA concentration (similar images for C_4S are shown in Figure S12). A reduced crystal aspect ratio in the presence of BSA is consistent with site-specific binding to {12-1} and/or {021} faces, which leads to the formation of diamond-shaped crystals (Figures 2E and 3B). Conversely, the increased crystal aspect ratio in the presence of C_4S (Figure

dx.doi.org/10.1021/ja410623q | J. Am. Chem. Soc. 2014, 136, 367−376

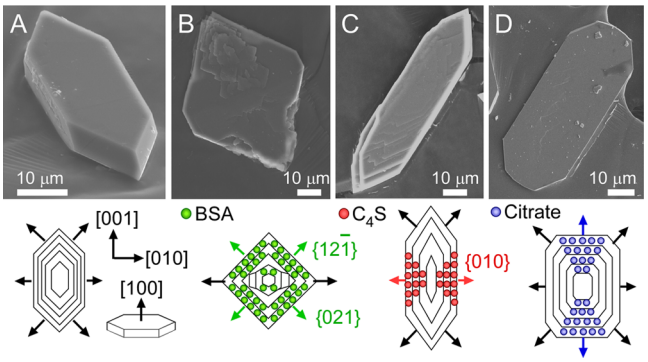

Figure 3. (A) COM control crystals exhibit an elongated hexagonal platelet morphology with a large basal (100) surface. SEM images reveal an average [001] length, [010] width, and [100] thickness of approximately 35 ± 6, 13 ± 2, and 9 ± 2 μm, respectively. Inhibitors that bind to COM crystals reduce growth rates normal to the face and alter crystal habit. We identified inhibitors that bind to specific faces of COM crystals: (B) BSA binds to {12-1} and {021} faces to produce diamond-shaped crystals; (B) C_4S binds to the (010) face to increase the [001] length of hexagonal platelets; and (D) citrate binds to steps on the (100) plane to reduce growth along the *c*-axis, which produces a quasi-rectangular crystal habit.

3C) suggests its preferential binding to the (010) face. We also observed that citrate produced rounded, rectangular-shaped crystals (Figure 3D), which is consistent with findings in the literature reporting citrate site-specificity for steps on the (100) surface that impedes growth along the *c*-axis.[9,27,28,44] SEM images and corresponding schematics in Figure 3 highlight differences in inhibitor specificity. The only inhibitor not shown in this series of images is Tf, which seemingly exhibits similar specificity as BSA, but has markedly less effect on the *c*/*b* aspect ratio of COM crystals (see Figure S9).

The general trend of COM aspect ratio as a function of inhibitor concentration (Figure 4A) is synonymous with Langmuir adsorption isotherms whereby inhibitor coverage on COM crystal surfaces reaches saturation at a threshold concentration, beyond which further increase in inhibitor concentration yields no additional morphological changes. Control crystals exhibit an aspect ratio of 2.8 ± 0.1. In the presence of C_4S, COM growth is reduced along the *b*-axis due to the preferential binding of C_4S to the (010) face. At low C_4S concentrations, there is a rapid increase in the COM crystal aspect ratio that plateaus at a value of 3.8 ± 0.1 around 5 μg/mL. Conversely, the preferential binding of BSA to apical tips results in a gradual reduction of the aspect ratio that reaches a minimum of 1.74 ± 0.08 at ∼20 μg/mL. Interestingly, we observed that the [001] length of COM crystals remained relatively constant during the transition from hexagonal to diamond-shaped crystals with increasing BSA concentration (Figure S8).

The data in Figure 4A reveal that Tf has a marginal impact on COM crystal habit; however, when we investigated the effect of higher Tf concentration we observed a decrease in crystal aspect ratio that reached a minimum plateau of 2.31 ± 0.08 at ∼70 μg/mL Tf (Figure S9). The reduced aspect ratio suggests that Tf preferentially binds to the apical {12-1} and/or {021} faces, similar to BSA. Our findings also revealed that Tf is a less effective inhibitor compared to C_4S and BSA (see Table 1), yet we observed that Tf has nearly the same impact on crystal thickness. Indeed, all three inhibitors produced an 80% reduction in the COM [100] dimension (Figure 4B) wherein

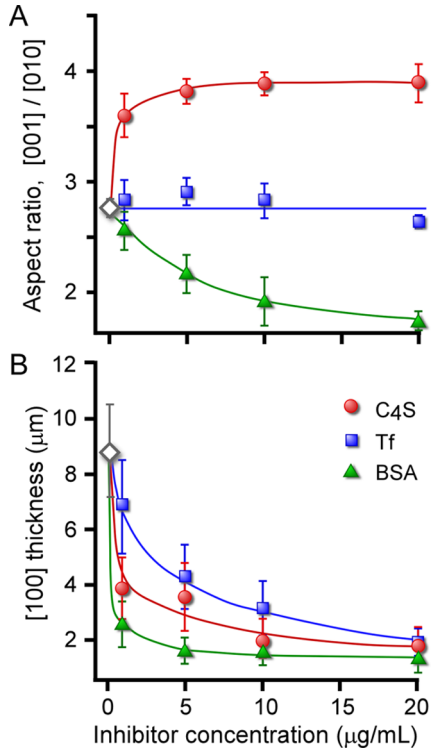

Figure 4. Changes in COM crystal dimension with increasing inhibitor concentration. (A) Aspect ratio (*c*/*b*) comparing the length-to-width of COM platelets along the [001] and [010] directions, respectively. C_4S site specificity for (010) faces increases the aspect ratio, whereas the preferentially binding of BSA to {12-1} and {021} faces produces diamond-shaped crystals. The effect of Tf in this concentration range is negligible; however, studies at higher concentration resulted in reduced aspect ratio (see Figure S9). (B) Measurements of COM crystal dimension along the [100] direction revealed an approximate 80% reduction in thickness for all three inhibitors. Data in (A) were measured from optical micrographs and are reported as the average of 200 crystals from 3 separate batches. Data in (B) were measured from SEM images and are reported as the average of 70 crystals from 3 separate batches. Error bars = 2 standard deviations.

the thickness monotonically decreased from 9 μm (control) to ∼2 μm with increasing inhibitor concentration.

AFM studies of COM growth have shown that steps emanating from screw dislocations on the (100) surface advance across the crystal plane as growth hillocks.[44,48] Burton, Cabrera, and Frank (BCF) derived a theoretical model of spiral growth predicting the rate of crystal growth normal to the basal face, $G_{[hkl]}$ (i.e., [100] direction for COM):

$$G_{[100]} = \frac{(v_i)_{hkl} h_{hkl}}{(y_i)_{hkl}} = \frac{h}{\tau} \quad (2)$$

where h_{hkl} is the height of (hkl) steps advancing along the (100) plane, y_i is the interstep distance, and v_i is the velocity of step advancement.[60,61] The subscript refers to the *i*th edge of growth hillocks, which advance across the surface in spiral patterns with a characteristic rotation time, τ. Measurements of COM [100] thickness (Figure 4B) are qualitatively consistent with this theoretical equation. Inhibitor binding to steps advancing across the basal surface increases τ of spiral growth (validated by *in situ* AFM studies of the (010) face in Figure 6), thereby reducing $G_{[100]}$ and the thickness of the COM platelet. Alternatively, a reduction in thickness may be attributed to

dx.doi.org/10.1021/ja410623q | J. Am. Chem. Soc. 2014, 136, 367−376

inhibitor binding to the (100) face, which would produce a similar effect by reducing hillock nucleation on the basal surface and step pinning of advancing hillocks. To examine this further, we used confocal microscopy to identify the preferential binding of fluorescently labeled BSA and Tf proteins to COM control crystals.

Fluorescence Imaging of Inhibitor Binding to COM Surfaces. Fluorescence microscopy is a useful tool for validating molecule/modifier site-specific interactions with (or incorporation within) crystals.[25,43,58,62−64] Here we used conventional fluorescence and confocal microscopy to examine the binding of BSA and Tf to bulk COM crystal surfaces. Fluorescence microscopy images of COM crystals incubated with AlexaFluor 633 labeled BSA and Tf are shown in Figure 5.

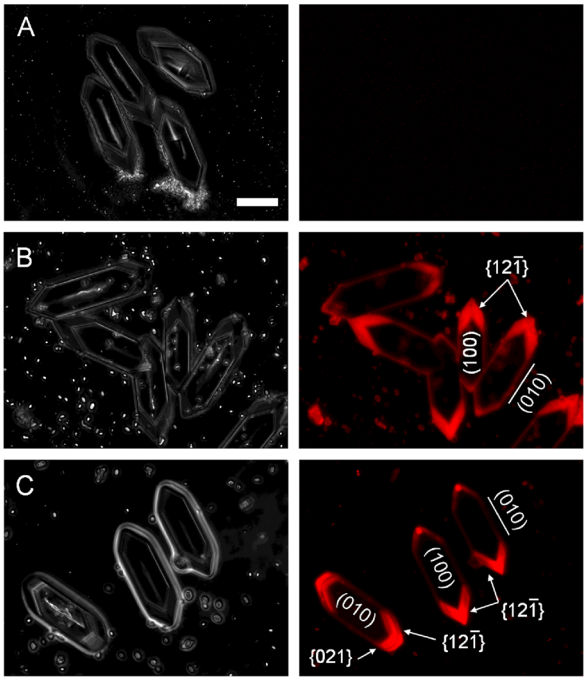

Figure 5. Fluorescence micrographs of crystals incubated with fluorescently labeled proteins. Left panels are brightfield images, and right panels are fluorescence images from the red channel (633 nm). Crystal surfaces are denoted as basal (100), apical {12-1} and {021}, and side (010) faces. (A) Control crystals exhibited no detectable autofluorescence in the red channel. (B) Crystals incubated with 20 μg/mL Alexa Fluor 647 Tf show selective binding to the apical tips. (C) Crystals incubated with 20 μg/mL Alexa Fluor 633 BSA show selective binding to both {12-1} and {021} faces. Neither Tf nor BSA showed specific adsorption on (100) and (010) surfaces. Scale bar = 25 μm (applies to all images).

COM crystals exhibited no autofluorescence in the red channel, but a very weak signal was detected in the green channel (Figure S22). For both proteins, the fluorescence is uniformly concentrated on the apical tips of COM crystals, which are defined by the {12-1} and {021} surfaces. Figure 5C clearly shows that BSA binds to both {12-1} and {021} surfaces. Moreover, it is evident that BSA and Tf do not preferentially bind to COM (100) or (010) surfaces, as previously postulated in the literature. As such, the reduced [100] dimension of COM crystals in Figure 4B is attributed to the BCF theory (eq 2).

Microscopic Validation of Inhibitor Specificity. AFM has proven to be a valuable tool for visualizing crystal growth and validating inhibition with near-molecular resolution.[11,36,65−67] COM crystals grow from spiral dislocations with parallelogram-shaped hillocks on the (010) face (Figure 6A) expressed by {12-1} and {021} steps. We used *in situ* AFM

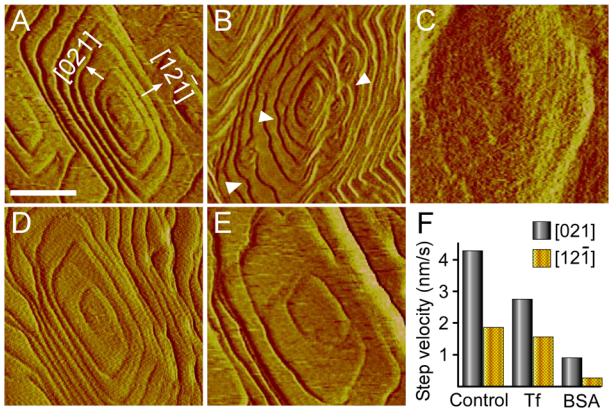

Figure 6. Snapshots from time-resolved *in situ* AFM imaging of hillock growth on the COM (010) face in supersaturated CaOx solutions. (A) Image of a control crystal with screw dislocations defined by {12-1} and {021} steps that advance across the surface. (B) Growth in the presence of 0.5 μg/mL C_4S results in step pinning (examples are highlighted by arrows). (C) Higher C_4S concentration (2.5 μg/mL) impedes step advance and produces roughened surfaces. Reintroduction of C_4S-free solution regenerates steps and hillock growth. (D) The presence of Tf decreases step advance in the [021] direction (see Movie S1). (E) The presence of BSA decreases step advance in both the [12-1] and [021] directions (see Movie S2). (F) Comparison of step velocities for Tf (2.5 μg/mL), BSA (0.25 μg/mL), and the control. All AFM images are presented in deflection mode with the same scale (scale bar = 1 μm).

to examine the effect of C_4S, BSA, and Tf on (010) hillock growth in supersaturated CaOx solutions. Measurements in the presence of C_4S revealed step pinning. These results are consistent with C_4S site specificity for (010) faces and theoretical models that predict steps advancing through adsorbates on terraces develop curvature (arrows in Figure 6B), which reduces localized supersaturation and impedes step motion. Higher C_4S concentration resulted in significant reduction of step growth that rendered the (010) surface rough and devoid of distinct steps (Figure 6C), analogous to the reported effects of OPN.[44] Reintroduction of inhibitor-free growth solution to the AFM liquid cell leads to step regeneration and the unabated growth of hillocks. The presence of Tf yielded elongated hillocks (Figure 6D) with reduced [021] step growth and a negligible effect on [12-1] step advance, whereas BSA significantly increased interstep distances (Figure 6E) and reduced step advancement in both the [021] and [12-1] directions. A comparison of step velocity, v, in Figure 6F shows a reduction in $v_{\{021\}}$ for both Tf and BSA and a reduction in $v_{\{12\text{-}1\}}$ for only BSA. It is evident from *in situ* AFM studies that BSA binds to both apical surfaces of COM crystals, while Tf exhibits site specificity for only the {021} face, which expresses the lowest surface area on bulk COM crystals. As such, AFM measurements are consistent with ISE and bulk crystallization studies identifying BSA as a more effective inhibitor relative to Tf.

Kinetics of COM Growth Inhibition. ISE measurements revealed a monotonic increase in the percent inhibition of COM crystallization with increasing inhibitor concentration

dx.doi.org/10.1021/ja410623q | J. Am. Chem. Soc. 2014, 136, 367−376

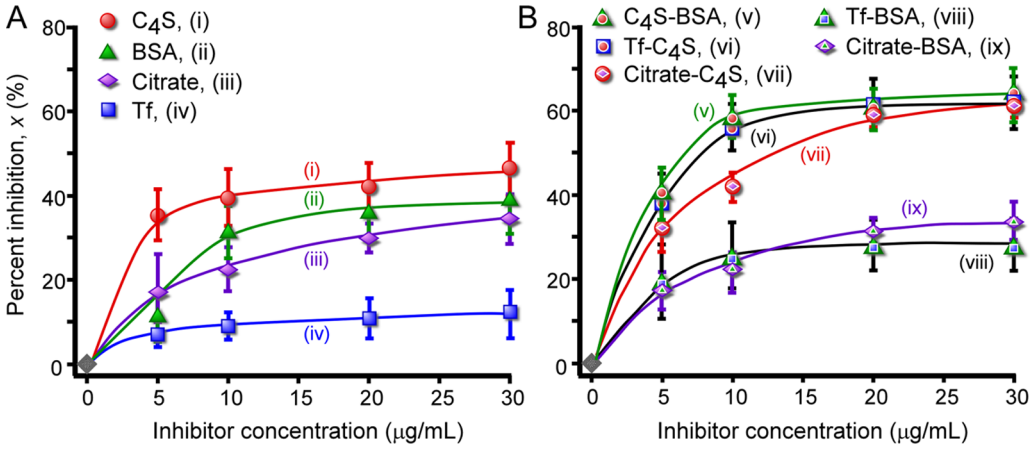

Figure 7. Kinetic studies of COM growth inhibition for single and binary combinations of inhibitors based on the rates of Ca^{2+} depletion from ISE measurements. (A) Single inhibitors exhibit the following trend in efficacy (from highest to lowest): C_4S > BSA ≥ citrate > Tf. (B) The binary combination C_4S-BSA produced the highest percent inhibition. Combinations Tf-C_4S and citrate-C_4S exhibit nearly identical behavior as the C_4S-BSA mixture. Conversely, Tf-BSA and citrate-BSA combinations are less effective. Concentrations for binary combinations refer to the total mass using equal weight percent of each inhibitor. Solid lines are guidelines; data are the average of three or more separate measurements; and error bars = 2 standard deviations.

(Figure 7). At some threshold concentration there is a plateau in the percent inhibition, which resembles a Langmuir adsorption curve (similar to the trends in crystal aspect ratio). Indeed, the threshold concentration in the kinetic data likely reflects the approximate point at which inhibitor coverage on COM crystal surfaces reaches thermodynamic equilibrium. We observed that C_4S is the most potent inhibitor based on its rapid increase in percent inhibition at concentrations <5 μg/mL. This is qualitatively consistent with the morphological changes observed in bulk crystallization studies (Figure 4A). By contrast, BSA is less potent and exhibits nearly twice the threshold concentration as C_4S. Kinetic studies revealed that Tf is a relatively weak inhibitor (x = 14 ± 3% at 70 μg/mL Tf), in agreement with AFM measurements of surface step growth. Analysis of citrate revealed that this benchmark inhibitor was slightly less potent than BSA and has a threshold concentration outside the range of this study (i.e., >30 μg/mL).

The inhibitors investigated in this study exhibit distinct site specificity for each principal surface of bulk COM crystals. This presents a unique opportunity to explore synergistic effects using inhibitor combinations. The use of two or more different inhibitors has the potential to impose either synergistic or antagonistic effects on crystal growth depending upon their cooperative interaction with COM faces. The use of drug combinations, or dose pairs, to suppress diseases, such as malaria[68] and cancer,[69] is a common approach in pharmacology and formulation design.[70] This method is amenable to crystal engineering via the judicious selection of modifier combinations that effectively tailor crystal properties (e.g., size and habit). Here we investigate inhibitor combinations using binary mixtures of BSA, C_4S, Tf, and citrate to assess their cooperative mode of action on the rate of COM growth. For all combinations considered, we used a 50/50 mixture (by mass) of total inhibitor concentration. We first analyzed pairings of inhibitors that interact with distinctly different faces of COM crystals. In all cases considered, the most potent inhibitor of the binary combination had a dominant effect on crystal morphology. For instance, the C_4S-BSA combination pairs inhibitors that bind to the (010) face and the apical faces, {12-1} and {021}. In this pairing, C_4S acts to increase crystal aspect ratio, while BSA has the opposite effect. Our studies revealed that the C_4S-BSA binary mixture resulted in COM crystals with increased aspect ratio (Figure S17), which suggests C_4S is the more influential mediator of crystal habit. ISE measurements of BSA-C_4S mixtures (Figure 7B) revealed an enhancement of x beyond what was achieved by either individual inhibitor (~70%), which can be attributed to the cooperative action of inhibitors targeting surfaces that contribute the fastest growth directions in bulk crystallization.

We also tested the combination of C_4S and Tf, which paired inhibitors with specificity for the (010) and {021} faces, respectively. Bulk crystallization revealed a monotonic increase in the c/b aspect ratio with increased C_4S-Tf concentration (Figure S17). This is again consistent with the most potent inhibitor, C_4S, having a more pronounced impact on crystal habit. ISE measurements of the binary mixture revealed an enhancement of x relative to each individual inhibitor (Figure 7B). Similar effects were observed for the combination of citrate and C_4S, which likewise paired two inhibitors with different site specificity. The results of this binary mixture were qualitatively similar to those reported by De Yoreo and co-workers using a combination of OPN and citrate. Their studies showed that the potent inhibitor, OPN, binds to steps presented on the COM (010) face,[44] while citrate binds to steps on the (100) plane (notably the intersection of the step riser and the underlying (100) terrace, thereby inhibiting step advancement along the c-axis).[48] In this same study, a binary mixture of OPN (5.5 nM) and citrate (0.1 mM) produced an additional 27% increase in percent inhibition beyond what was achieved by only OPN.[28]

The binary combinations C_4S-BSA and C_4S-citrate pair two efficacious inhibitors; therefore, it is reasonable to expect that these combinations will yield a higher percent inhibition than either individual inhibitor. Interestingly, the combination Tf-C_4S, which pairs a weak and potent inhibitor, respectively, resulted in an enhanced x comparable to mixtures of two potent inhibitors. The combination BSA-citrate, which pairs two effective inhibitors with different site specificity, yielded virtually no enhancement of x. Likewise, the combination Tf-BSA resulted in negligible synergy owing to their overlapping

dx.doi.org/10.1021/ja410623q | J. Am. Chem. Soc. 2014, 136, 367−376

site specificity, which likely engenders competitive binding to COM {021} crystal surfaces.

In addition to ISE measurements, we also performed dynamic light scattering (DLS) analyses of C_4S, BSA, Tf, and mixtures thereof in oxalate-free growth solutions to ensure that the observed effects of binary combinations were not attributed to interactions between inhibitors in solution through the formation of binary species. The impact of such species could be two-fold: (i) The formation of binary complexes act as a single, more potent inhibitor; or (ii) the formation of aggregates reduces available inhibitor concentration in COM growth solutions. The hydrodynamic diameters measured by DLS, however, showed no evidence of increased particle size that would be indicative of either aggregate or complex formation (Figure S18).

A rigorous quantitative analysis of the cooperative effects of COM growth inhibitors was performed by the construction of isobolograms (Figure 8), which is a technique commonly employed in drug testing. This graphical tool plots the equipotency sum of inhibitor concentration. Isobolograms for the C_4S-BSA and Tf-BSA combinations are presented in Figure 8, while those for Tf-C_4S, citrate-BSA, and citrate-C_4S are provided in Figure S20. The graphical interpretation of these plots is as follows. Binary combinations (solid symbols) that lie below the solid lines connecting data for single inhibitors (open symbols) signify synergism; those that lie near or along the solid line represent additive effects; and those that are above the line indicate an antagonistic effect. Using data in Figure 7, we calculated the combination index (CI):

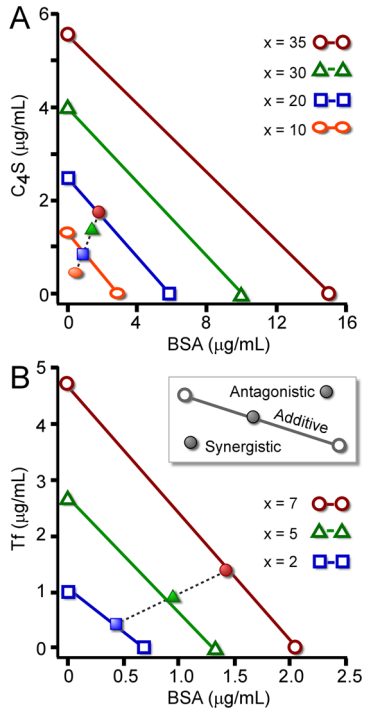

Figure 8. Classic isobolograms for (A) C_4S-BSA and (B) Tf-BSA combinations. Solid lines with open symbols represent an additive effect (CI = 1) for different percent inhibition, x. Closed symbols are combinations of binary mixtures. Data in panel A reveal combinations that lie below the solid lines, signifying synergism, whereas data in panel B are close to the lines and nearly additive. Isobolograms for Tf-C_4S, BSA-citrate, and C_4S-citrate combinations are provided in Figure S20.

$$\mathrm{CI} = \frac{(D)_1}{(D_x)_1} + \frac{(D)_2}{(D_x)_2} \tag{3}$$

where $(D)_i$ is the "dose" (i.e., concentration, μg/mL) of species i in the binary mixture that inhibits COM crystallization by x (percent inhibition), and $(D_x)_i$ is the concentration of species i used as an individual inhibitor to achieve the same percent inhibition as the binary mixture. This mathematical expression facilitates the comparison of inhibitor combinations that display synergism (CI < 1), additivity (CI = 1), or antagonism (CI > 1). This so-called Chou–Talalay combination index theorem[71] was introduced as a means of quantifying the effect of drug combinations (see the review by Chou).[72] Here we use this theorem to characterize the effects of COM inhibitor pairings, which to our knowledge is the first application of the CI analysis in studies of crystal engineering.

The CI values for each inhibitor combination as a function of increasing x are shown in Table 2 and Figure S21, along with their corresponding weight-averaged values, CI_{wt}. Semiquantitative ranges of CI defined in the literature label the effects in categories, such as strong synergism, synergism, moderate synergism, nearly additive, slight antagonism, and moderate antagonism. Interestingly, we observe COM inhibitor pairings that span nearly all ranges. The most synergistic effects occurred with C_4S-Tf and C_4S-BSA, which exhibit nearly identical CI value. In contrast, the pairing C_4S-citrate was less effective. The pairing of inhibitors with similar site specificity, Tf-BSA, produced a nearly additive effect, while the citrate-BSA binary combination was slightly antagonistic. In the latter pairing, both inhibitors interact with steps on triangular hillocks within the basal (100) plane (illustrated in Figure 1A). As shown in Figure 3, citrate reduces the surface area of apical tips, which thereby decreases the available surface area for BSA adsorption. As such, the concerted binding of these two inhibitors to (100) growth hillocks produces an antagonistic effect, which is a unique finding for COM growth inhibition with potentially broader implications for crystal design. Notably, this result highlights the importance of selecting an appropriate combination to achieve the desired effect.

CONCLUSION

In summary, we have examined the specificity and resulting influence of biomolecular inhibitors on the crystallization of COM, which is a model system of calcification with specific relevance for pathological mineralization. We analyzed three natural inhibitors of COM crystallization using a combination of microscopy techniques to determine their specificity for different faces of COM crystals and to quantify their impact on crystal habit and growth rate. We have conclusively shown that chondroitin sulfate and serum albumin preferentially bind to COM {010} and {12-1}/{021} faces, respectively. These site-specific interactions resulted in distinct morphological modifications of COM crystal aspect ratio. Transferrin preferentially binds to {021} faces and produced only moderate changes in crystal habit. Kinetic studies of COM bulk crystallization revealed marked differences in inhibitor efficacy. Using the CI theorem, we showed that inhibitor pairings with either similar or different site specificity yielded a range of effects spanning synergism to antagonism.

In a broader context, the combination effects observed here may in fact elude to a more widespread mechanism of biomolecules in living systems that modulate pathological mineralization. This generalized mode of action offers new

dx.doi.org/10.1021/ja410623q | J. Am. Chem. Soc. 2014, 136, 367–376

Table 2. Cooperative Effects of Binary Inhibitor Combinations

	combination index, CI				
x (%)	Tf-BSA	Tf-C_4S	BSA-C_4S	BSA-citrate	citrate-C_4S
2	1.09	0.59	0.68	1.03	0.78
5	1.08	0.52	0.64	1.05	0.76
7	0.99	0.48	0.58	1.07	0.75
10	0.94	0.44	0.54	1.07	0.77
20			0.51	1.09	0.73
30			0.51	1.21	0.69
35			0.44		
CI_{wt} [a]	1.00	0.48	0.52	1.11	0.74
effect [b]	nearly additive	synergism	synergism	slight antagonism	moderate synergism

[a] $CI_{wt} = \sum_{i=1}^{N} i \cdot CI(i) / \sum_{i=1}^{N} i$, where i = 1, 2, ..., N goes from lowest to highest x. [b] Based on categories defined by Chou [72] for ranges of CI.

approaches for the rational design of combination therapies aimed at inhibiting COM crystallization in renal stone disease. An improved understanding of crystal inhibition mechanisms at the molecular level may provide insights for the design of improved stone therapies. Indeed, such knowledge could allow production of inhibitors that potentiate the natural inhibitors present in urine or lead to production of inhibitors that work in tandem to provide synergistic activity while minimizing the dose needed of either drug to minimize potential side effects.

Designing biomimetic molecules capable of emulating *in vivo* growth inhibition may also provide routes in crystal engineering to tailor physical properties of materials that otherwise could not be achieved through more conventional synthetic methods. Indeed, a single inhibitor or multiple inhibitors acting cooperatively can be used to tune the size and habit of virtually any crystalline material. Designing site-specific inhibitors of crystals hinges upon a molecular level understanding of inhibitor−crystal interactions and the stereochemical source of their molecular recognition. To this end, techniques capable of probing interfacial phenomena, such as AFM and molecular modeling, will be invaluable tools to elucidate inhibitor binding to crystal surfaces. Significant advancements over the years have led to the identification of inhibitors and their respective role(s) in modulating crystallization. The outcome of these and future studies can potentially impact diverse areas spanning materials design and synthesis to pharmaceuticals.

■ ASSOCIATED CONTENT

Supporting Information

Details of protein structures and CD measurements; ISE calibration and data for C_4S and Tf; analysis of albumin sources (human and bovine); bulk crystallization studies of COM crystal size and number density; AFM measurements of COM (100) surface topography and step heights; Movies S1 and S2 of AFM *in situ* growth; DLS measurements of inhibitor size; combination studies (ISE and bulk crystallization); and additional images from scanning confocal microscopy. This material is available free of charge via the Internet at http://pubs.acs.org.

■ AUTHOR INFORMATION

Corresponding Author

jrimer@central.uh.edu

Notes

The authors declare no competing financial interest.

■ ACKNOWLEDGMENTS

We acknowledge funding from the National Science Foundation (DMR Awards 1207441 and 1207411) and the Welch Foundation (Grant E-1794). We are grateful to Ricardo Sosa for help with bulk crystallization assays, John Kwak with SCM, and Dr. John Craft with CD measurements.

■ REFERENCES

(1) Suzuki, M.; Saruwatari, K.; Kogure, T.; Yamamoto, Y.; Nishimura, T.; Kato, T.; Nagasawa, H. *Science* **2009**, *325*, 1388.
(2) Nancollas, G. H.; Tang, R.; Phipps, R. J.; Henneman, Z.; Gulde, S.; Wu, W.; Mangood, A.; Russell, R. G. G.; Ebetino, F. H. *Bone* **2006**, *38*, 617.
(3) Aizenberg, J.; Weaver, J. C.; Thanawala, M. S.; Sundar, V. C.; Morse, D. E.; Fratzl, P. *Science* **2005**, *309*, 275.
(4) Kroger, N.; Deutzmann, R.; Sumper, M. *Science* **1999**, *286*, 1129.
(5) Graether, S. P.; Kuiper, M. J.; Gagne, S. M.; Walker, V. K.; Jia, Z. C.; Sykes, B. D.; Davies, P. L. *Nature* **2000**, *406*, 325.
(6) Chen, C. L.; Qi, J. H.; Zuckermann, R. N.; DeYoreo, J. J. *J. Am. Chem. Soc.* **2011**, *133*, 5214.
(7) Huang, M. L.; Ehre, D.; Jiang, Q.; Hu, C. H.; Kirshenbaum, K.; Ward, M. D. *Proc. Natl. Acad. Sci. U.S.A.* **2012**, *109*, 19922.
(8) Weissbuch, I.; Leiserowitz, L. *Chem. Rev.* **2008**, *108*, 4899.
(9) De Yoreo, J. J.; Qiu, S. R.; Hoyer, J. R. *Am. J. Physiol. Renal Physiol.* **2006**, *291*, F1123.
(10) Farmanesh, S.; Chung, J.; Chandra, D.; Sosa, R. D.; Karande, P.; Rimer, J. D. *J. Cryst. Growth* **2013**, *373*, 13.
(11) Rimer, J. D.; An, Z. H.; Zhu, Z. N.; Lee, M. H.; Goldfarb, D. S.; Wesson, J. A.; Ward, M. D. *Science* **2010**, *330*, 337.
(12) Addadi, L.; Berkovitchyellin, Z.; Weissbuch, I.; Vanmil, J.; Shimon, L. J. W.; Lahav, M.; Leiserowitz, L. *Angew. Chem., Int. Ed. Engl.* **1985**, *24*, 466.
(13) Berkovitchyellin, Z.; Vanmil, J.; Addadi, L.; Idelson, M.; Lahav, M.; Leiserowitz, L. *J. Am. Chem. Soc.* **1985**, *107*, 3111.
(14) Lupulescu, A. I.; Kumar, M.; Rimer, J. D. *J. Am. Chem. Soc.* **2013**, *135*, 6608.
(15) Lupulescu, A. I.; Rimer, J. D. *Angew. Chem., Int. Ed.* **2012**, *51*, 3345.
(16) Mavredaki, E.; Neville, A.; Sorbie, K. S. *Cryst. Growth Des.* **2011**, *11*, 4751.
(17) Keene, E. C.; Evans, J. S.; Estroff, L. A. *Cryst. Growth Des.* **2010**, *10*, 1383.
(18) Li, H. Y.; Estroff, L. A. *J. Am. Chem. Soc.* **2007**, *129*, 5480.
(19) Gower, L. B. *Chem. Rev.* **2008**, *108*, 4551.
(20) Huang, W. C.; Lyu, L. M.; Yang, Y. C.; Huang, M. H. *J. Am. Chem. Soc.* **2012**, *134*, 1261.
(21) Chen, L.; Xie, A.; Jia, R.; Shen, Y.; Tang, W.; Li, C. *Cryst. Res. Technol.* **2007**, *42*, 881.
(22) Khan, S. R. *Urol. Int.* **1997**, *59*, 59.
(23) Canales, B. K.; Anderson, L.; Higgins, L.; Slaton, J.; Roberts, K. P.; Liu, N. T.; Monga, M. *J. Endourol.* **2008**, *22*, 1161.

(24) Dussol, B.; Geider, S.; Lilova, A.; Leonetti, F.; Dupuy, P.; Daudon, M.; Berland, Y.; Dagorn, J. C.; Verdier, J. M. *Urol. Res.* **1995**, *23*, 45.
(25) Taller, A.; Grohe, B.; Rogers, K. A.; Goldberg, H. A.; Hunter, G. K. *Biophys. J.* **2007**, *93*, 1768.
(26) Hirose, M.; Tozawa, K.; Okada, A.; Hamamoto, S.; Higashibata, Y.; Gao, B.; Hayashi, Y.; Shimizu, H.; Kubota, Y.; Yasui, T.; Kohri, K. *Urol. Res.* **2012**, *40*, 121.
(27) Grohe, B.; O'Young, J.; Langdon, A.; Karttunen, M.; Goldberg, H. A.; Hunter, G. K. *Cells Tissues Organs* **2011**, *194*, 176.
(28) Wang, L. J.; Zhang, W.; Qiu, S. R.; Zachowicz, W. J.; Guan, X. Y.; Tang, R. K.; Hoyer, J. R.; De Yoreo, J. J.; Nancollas, G. H. *J. Cryst. Growth* **2006**, *291*, 160.
(29) Jung, T.; Sheng, X. X.; Choi, C. K.; Kim, W. S.; Wesson, J. A.; Ward, M. D. *Langmuir* **2004**, *20*, 8587.
(30) Kleinman, J. G.; Alatalo, L. J.; Beshensky, A. M.; Wesson, J. A. *Kidney Int.* **2008**, *74*, 919.
(31) Akyol, E.; Bozkurt, A.; Oner, M. *Polymer. Adv. Tech.* **2006**, *17*, 58.
(32) Akyol, E.; Oner, M. *J. Cryst. Growth* **2007**, *307*, 137.
(33) Thurgood, L. A.; Cook, A. F.; Sorensen, E. S.; Ryall, R. L. *Urol. Res.* **2010**, *38*, 357.
(34) Hug, S.; Grohe, B.; Jalkanen, J.; Chan, B.; Galarreta, B.; Vincent, K.; Lagugne-Labarthet, F.; Lajoie, G.; Goldberg, H. A.; Karttunen, M.; Hunter, G. K. *Soft Matter* **2012**, *8*, 1226.
(35) Tazzoli, V.; Domeneghetti, C. *Am. Mineral.* **1980**, *65*, 327.
(36) Wang, L. J.; Qiu, S. R.; Zachowicz, W.; Guan, X. Y.; DeYoreo, J. J.; Nancollas, G. H.; Hoyer, J. R. *Langmuir* **2006**, *22*, 7279.
(37) Fleming, D. E.; van Bronswijk, W.; Ryall, R. L. *Clin. Sci.* **2001**, *101*, 159.
(38) Coe, F. L.; Nakagawa, Y.; Asplin, J.; Parks, J. H. *Miner. Electrolyte Metab.* **1994**, *20*, 378.
(39) Sheng, X. X.; Jung, T. S.; Wesson, J. A.; Ward, M. D. *Proc. Natl. Acad. Sci. U.S.A.* **2005**, *102*, 267.
(40) Liu, J. F.; Jiang, H. D.; Liu, X. Y. *J. Phys. Chem. B* **2006**, *110*, 9085.
(41) Shirane, Y.; Kurokawa, Y.; Miyashita, S.; Komatsu, H.; Kagawa, S. *Urol. Res.* **1999**, *27*, 426.
(42) Wang, L. J.; Guan, X. Y.; Tang, R. K.; Hoyer, J. R.; Wierzbicki, A.; De Yoreo, J. J.; Nancollas, G. H. *J. Phys. Chem. B* **2008**, *112*, 9151.
(43) Langdon, A.; Wignall, G. R.; Rogers, K.; Sorensen, E. S.; Denstedt, J.; Grohe, B.; Goldberg, H. A.; Hunter, G. K. *Calcif. Tissue Int.* **2009**, *84*, 240.
(44) Qiu, S. R.; Wierzbicki, A.; Orme, C. A.; Cody, A. M.; Hoyer, J. R.; Nancollas, G. H.; Zepeda, S.; De Yoreo, J. J. *Proc. Natl. Acad. Sci. U.S.A.* **2004**, *101*, 1811.
(45) Kazemi-Zanjani, N.; Chen, H. H.; Goldberg, H. A.; Hunter, G. K.; Grohe, B.; Lagugne-Labarthet, F. *J. Am. Chem. Soc.* **2012**, *134*, 17076.
(46) Chan, B. P. H.; Vincent, K.; Lajoie, G. A.; Goldberg, H. A.; Grohe, B.; Hunter, G. K. *Colloids Surf. B* **2012**, *96*, 22.
(47) An, Z. H.; Lee, S.; Oppenheimer, H.; Wesson, J. A.; Ward, M. D. *J. Am. Chem. Soc.* **2010**, *132*, 13188.
(48) Qiu, S. R.; Wierzbicki, A.; Salter, E. A.; Zepeda, S.; Orme, C. A.; Hoyer, J. R.; Nancollas, G. H.; Cody, A. M.; De Yoreo, J. J. *J. Am. Chem. Soc.* **2005**, *127*, 9036.
(49) Weaver, M. L.; Qiu, S. R.; Hoyer, J. R.; Casey, W. H.; Nancollas, G. H.; De Yoreo, J. J. *J. Cryst. Growth* **2007**, *306*, 135.
(50) Guo, S. W.; Ward, M. D.; Wesson, J. A. *Langmuir* **2002**, *18*, 4284.
(51) Hoyer, J. R.; Asplin, J. R.; Otvos, L. *Kidney Int.* **2001**, *60*, 77.
(52) Pampena, D. A.; Robertson, K. A.; Litvinova, O.; Lajoie, G.; Goldberg, H. A.; Hunter, G. K. *Biochem. J.* **2004**, *378*, 1083.
(53) Azzopardi, P. V.; O'Young, J.; Lajoie, G.; Karttunen, M.; Goldberg, H. A.; Hunter, G. K. *PLoS One* **2010**, 5.
(54) Grohe, B.; Chan, B. P. H.; Sorensen, E. S.; Lajoie, G.; Goldberg, H. A.; Hunter, G. K. *Urol. Res.* **2011**, *39*, 327.
(55) Weaver, M. L.; Qiu, S. R.; Hoyer, J. R.; Casey, W. H.; Nancollas, G. H.; De Yoreo, J. J. *Calcif. Tissue Int.* **2009**, *84*, 462.
(56) Wesson, J. A.; Worcester, E. M.; Kleinman, J. G. *J. Urol.* **2000**, *163*, 1343.
(57) Elhadj, S.; Salter, E. A.; Wierzbicki, A.; De Yoreo, J. J.; Han, N.; Dove, P. M. *Cryst. Growth Des.* **2006**, *6*, 197.
(58) Cook, A. F.; Grover, P. K.; Ryall, R. L. *BJU Int.* **2009**, *103*, 826.
(59) Gul, A.; Rez, P. *Urol. Res.* **2007**, *35*, 63.
(60) Lovette, M. A.; Browning, A. R.; Griffin, D. W.; Sizemore, J. P.; Snyder, R. C.; Doherty, M. F. *Ind. Eng. Chem. Res.* **2008**, *47*, 9812.
(61) Snyder, R. C.; Doherty, M. F. *Proc. R. Soc. A* **2009**, *465*, 1145.
(62) Grohe, B.; O'Young, J.; Ionescu, D. A.; Lajoie, G.; Rogers, K. A.; Karttunen, M.; Goldberg, H. A.; Hunter, G. K. *J. Am. Chem. Soc.* **2007**, *129*, 14946.
(63) Chien, Y. C.; Masica, D. L.; Gray, J. J.; Nguyen, S.; Vali, H.; McKee, M. D. *J. Biol. Chem.* **2009**, *284*, 23491.
(64) Kahr, B.; Gurney, R. W. *Chem. Rev.* **2001**, *101*, 893.
(65) Cho, K. R.; Salter, E. A.; De Yoreo, J. J.; Wierzbicki, A.; Elhadj, S.; Huang, Y.; Qiu, S. R. *CrystEngComm* **2013**, *15*, 54.
(66) Perrin, C. M.; Dobish, M. A.; Van Keuren, E.; Swift, J. A. *CrystEngComm* **2011**, *13*, 1111.
(67) Perrin, C. M.; Swift, J. A. *CrystEngComm* **2012**, *14*, 1709.
(68) Kelly, J. X.; Smilkstein, M. J.; Brun, R.; Wittlin, S.; Cooper, R. A.; Lane, K. D.; Janowsky, A.; Johnson, R. A.; Dodean, R. A.; Winter, R.; Hinrichs, D. J.; Riscoe, M. K. *Nature* **2009**, *459*, 270.
(69) Pegram, M.; Hsu, S.; Lewis, G.; Pietras, R.; Beryt, M.; Sliwkowski, M.; Coombs, D.; Baly, D.; Kabbinavar, F.; Slamon, D. *Oncogene* **1999**, *18*, 2241.
(70) Karande, P.; Jain, A.; Mitragotri, S. *Nat. Biotechnol.* **2004**, *22*, 192.
(71) Chou, T. C.; Talalay, P. *Adv. Enzyme Regul.* **1984**, *22*, 27.
(72) Chou, T. C. *Pharmacol. Rev.* **2006**, *58*, 621.